

Article

# Path-Guided Finite-Time Formation Control of Nonholonomic Mobile Robots Based on an Extended State Observer

Yanyan Fan <sup>1</sup>, Zhenlin Jin <sup>1,\*</sup>, Xiaoyuan Luo <sup>2</sup> , Shaobao Li <sup>2</sup> and Baosu Guo <sup>1</sup><sup>1</sup> School of Mechanical Engineering, Yanshan University, Qinhuangdao 066004, China<sup>2</sup> School of Electrical Engineering, Yanshan University, Qinhuangdao 066004, China

\* Correspondence: zljn@ysu.edu.cn

**Abstract:** In this paper, we study the finite-time formation control problem of uncertain nonholonomic mobile robots following a parameterized path. A path-guided formation control scheme based on an extended state observer is proposed. To compensate for unmeasured velocities and disturbances simultaneously, a third-order fast finite-time extended state observer (FFTESO) is proposed. Then, a distributed formation control solution is developed to achieve the kinematic and dynamic system coordination control of the nonholonomic mobile robots. For the kinematic system control, a path-parameter-updating law is developed for a virtual leader, and the desired linear velocity and heading angle are developed for the mobile robots. For the kinetic control, an anti-disturbance control protocol is designed based on the estimated signals. The salient features of the proposed algorithms lie in that the estimations of disturbances and unmeasured velocities are achieved against the system's nonholonomic constraints, and the path following the control and cooperative control is synthesized together for path-guided formation, which reduces the complexity of the controller design. Finally, simulation studies are conducted to demonstrate the effectiveness of the proposed algorithm.

**Keywords:** nonholonomic mobile robot; finite-time convergence; formation control; path-guided; extended state observer



**Citation:** Fan, Y.; Jin, Z.; Luo, X.; Li, S.; Guo, B. Path-Guided Finite-Time Formation Control of Nonholonomic Mobile Robots Based on an Extended State Observer. *Appl. Sci.* **2022**, *12*, 9281. <https://doi.org/10.3390/app12189281>

Academic Editor: Oscar Reinoso García

Received: 4 August 2022

Accepted: 12 September 2022

Published: 16 September 2022

**Publisher's Note:** MDPI stays neutral with regard to jurisdictional claims in published maps and institutional affiliations.



**Copyright:** © 2022 by the authors. Licensee MDPI, Basel, Switzerland. This article is an open access article distributed under the terms and conditions of the Creative Commons Attribution (CC BY) license (<https://creativecommons.org/licenses/by/4.0/>).

## 1. Introduction

The formation control of multiple mobile robots has recently become a hot research issue with the development of the technology on multi-agent systems and its applications on robots [1–3]. The objective of formation control is to develop control algorithms for a group of robots such that a predefined formation shape can be achieved to perform some tasks cooperatively. Multi-robot formation control has wide applications in military and civil areas, such as cooperation transportation [4], search and rescue [5], surveillance [6], etc., due to its advantages in communication and collaboration.

The main purpose of the path-guided multi-robot formation is to make the mobile robots keep the desired formation and move along a parameterized path (called the geometric task). For example, the virtual structure approach was used to achieve the desired formation by considering the formation as a rigid body, and the model predictive control was employed to optimize the velocity of the virtual robot [7]. Besides the studies on geometric tasks, many research studies have focused on specifying the desired speed for the path parameter (called the dynamic task). Its advantage is that the path parameter can be treated as an additional degree of freedom. In [8], the path-following time-varying formation control problem was studied for a group of mobile robots with a unicycle-type kinematic model by designing a path-parameter-updating law. However, the control law is centralized. Then, an improved law for the distributed virtual-structure-based path-following formation control was developed in [9], where both the path following of individual robots and the desired formation pattern were achieved. In [10], based on the virtual structure approach, a multi-robot formation control method was studied in which multiple mobile robots moved along a parameterized path with obstacles. In [11],

a path-following control and formation maintenance problem was solved for multiple mobile robots that were subjected to a prescribed performance level by using the backstepping technique and tan-type barrier Lyapunov functions. In [12], the path-following and formation control of multiple mobile robots were achieved by using a virtual structure algorithm and designing a proper path-parameter-updating law. It should be noted that the methods proposed in [10–12] only focused on the formation control at the kinematic level, but the dynamic control was not considered. In [13], the path-following control problem of multiple uncertain mobile robots with performance constraints was studied, and the proposed strategy was extended to the formation control of multiple unicycle-type robots. The above-mentioned control algorithms in [7–13] dealt with the path-guided formation control problem of multi-robot systems by assigning a desired path for each mobile robot and transforming the formation control problem into a multi-path-following problem without considering the coordination of the mobile robots. In practical engineering, the multi-path-guided formation may cause a heavy computational burden due to the constantly updating of path parameters once the formation pattern changes, thus leading to the instability of the system.

It should be noted that the dynamic control methods of the multiple mobile robot formation in the aforementioned works [8,9,13] are constrained to an accurate dynamic model and do not consider the effect of external disturbances on the stability of the system. To improve the robustness of the formation control by considering the effect of model uncertainties and external disturbances, a great number of methods have been proposed. In [14], an integral sliding mode controller was proposed to deal with external disturbances and achieve the formation control of multiple mobile robots. In [15], a terminal sliding mode control law was proposed to deal with model uncertainties at the dynamic level and external disturbances. In [16], a Q-learning-based adaptive sliding mode controller was proposed for the formation control of multiple mobile robots. However, the chattering of the sliding mode control in [15–17] causes serious wear to the mobile robots. A radial basis function neural network was used to approximate the model uncertainties of multiple mobile robots in [18,19]. A fixed-time disturbance observer was proposed in [20] to estimate external disturbances, and a leader–follower formation controller was developed for multi-robot systems. The active disturbance rejection control (ADRC) is a widely used method to compensate for unknown disturbances, which was introduced for the robust control of the dynamic systems in [21] and nonlinear systems in [22]. Considering the ADRC of mobile robotics, a survey summarized the mainstream control strategies and pointed out the advantages of the ADRC on the robust control of mobile robots [23]. The above works show the advantages of the ADRC in the robust control of mobile robots. As the core of the ADRC, the extended state observer is used to estimate the total disturbances of the system. In [24–32], an extended state observer was applied only based on the dynamics of mobile robots. However, if the velocity is unmeasurable, the proposed extended state observer is unavailable because of having the characteristic of nonholonomic constraints. Moreover, the application of the extended state observer to the path-guided formation control of multiple mobile robots is meaningful but rarely studied.

Motivated by the aforementioned discussions, in this paper, we investigate the output-feedback-based path-guided finite-time formation control of nonholonomic mobile robots. Firstly, a fast finite-time ESO (FFTESO) is proposed to estimate the unmeasured velocities and disturbances. Then, a formation control scheme including the kinematic and dynamic control laws is proposed. For the kinematic control law, a path-parameter-updating law is developed for a virtual leader, and the desired linear velocity and heading angle are designed for the mobile robots. For the dynamic control law, an anti-disturbance control protocol is designed based on the estimated signals. The main contributions of this work are as follows:

- (1) A fast finite-time extended state observer is developed to estimate the unmeasured velocities and disturbances, thus overcoming nonholonomic constraints while improving the observation accuracy and speed;

- (2) A finite-time formation control scheme is proposed for the kinematic and dynamic control of multiple mobile robots. The proposed path-guided formation controller integrates the path-following control and formation control to relax the assumption of a globally known parameterized path, which is needed in [10–13];
- (3) A single-path-updating law is developed to drive the formation to follow the parameterized path with the assigned speed. Compared with the multi-path-updating law in [7–13], the proposed single-path-updating law reduces computing and communication resources.

The rest of this article is organized as follows: The preliminaries are introduced in Section 2. In Section 3, the finite-time extended state observer, the double closed-loop kinematic controller, and the output-feedback-based dynamic controller are developed. In Section 4, the stability analysis of the closed-loop system is presented. In Section 5, simulation studies are conducted to demonstrate the effectiveness of the proposed algorithm. Finally, Section 5 concludes this paper.

Notations:  $\mathbb{R}$  is the set of real numbers.  $|\cdot|$  represents the absolute value of a scalar, and  $\|\cdot\|$  is the Euclidean norm of a vector. Given a vector  $e = [e_1, e_2, \dots, e_p]^T$ ,  $\text{sgn}(e) = [\text{sgn}(e_1), \text{sgn}(e_2), \dots, \text{sgn}(e_p)]^T$  and  $\text{sig}^\alpha(e) = [|e_1|^\alpha \text{sgn}(e_1), |e_2|^\alpha \text{sgn}(e_2), \dots, |e_p|^\alpha \text{sgn}(e_p)]^T$ , where  $\text{sgn}(\cdot)$  is the signum function,  $(\cdot)^T$  is the transpose of a vector or a matrix.  $\lambda_{\min}(\cdot)$  is the minimum eigenvalue of a matrix.

## 2. Preliminaries

### 2.1. Graph Theory

Consider a system consisting of  $N$  mobile robots (labeled as  $n_1, n_2, \dots, n_N$ ) and one virtual leader (labeled as  $n_0$ ). The communication topology of the multi-robot system is described by a directed graph  $\mathcal{G} = (\mathcal{V}, \mathcal{E})$  with a set of mobile robots  $\mathcal{V} = \{n_0, n_1, \dots, n_N\}$  and a set of edges  $\mathcal{E} \subseteq \mathcal{V} \times \mathcal{V}$ . The edge  $(i, j) \in \mathcal{E}$  means node  $i$  can obtain information from node  $j$ , and node  $j$  is a neighbor of node  $i$ . The set of neighbors of node  $i$  is denoted by  $\mathcal{N}_i = \{j \in \mathcal{V} \mid (i, j) \in \mathcal{E}\}$ . A directed path from node  $i_1$  to node  $i_s$  is a sequence of ordered directed edges consisting of  $\{(i_1, i_2), (i_2, i_3), \dots, (i_{s-1}, i_s)\}$ . For the  $N$  following mobile robots, the subgraph  $\bar{\mathcal{G}}$  is used to describe the communication topology among the robots labeled as  $n_1, n_2, \dots, n_N$ . The adjacency matrix of the graph  $\mathcal{G}$  is denoted as  $\mathcal{A}(\mathcal{G}) = [a_{ij}]$ , where  $a_{ij} = 1$  if  $(i, j) \in \mathcal{E}$  and  $a_{ij} = 0$ , if otherwise. The Laplacian matrix  $\mathcal{L} = [l_{ij}]$  is defined as  $l_{ii} = \sum_{j=1, j \neq i}^N a_{ij}$  and  $l_{ij} = -a_{ij}, i \neq j, i, j = 1, 2, \dots, N$ . In this paper, suppose that the virtual leader has none of the following robots' information, i.e.,  $a_{0i} = 0, i = 1, 2, \dots, N$ , and at least one of the following robots can access the information of the virtual leader. Let  $\bar{\mathcal{L}} \in \mathbb{R}^{N \times N}$  be the Laplacian matrix of subgraph  $\bar{\mathcal{G}}$ ,  $B \in \mathbb{R}^{N \times N} = \text{diag}\{a_{10}, a_{20}, \dots, a_{N0}\}$  and  $H = \bar{\mathcal{L}} + B$ . The following assumption is needed:

**Assumption 1.** *There exists a directed spanning tree with the virtual leader as the root in graph  $\mathcal{G}$ .*

### 2.2. Problem Formulation

As shown in Figure 1,  $O - X_E Y_E$  is the global coordinate frame, and  $C - X_B Y_B$  is the body-fixed coordinate frame. The mobile robots with two actuated wheels are controlled to keep the desired formation pattern and follow a desired path by exchanging information with their neighbor robots. According to [25], the dynamics of the  $i$ th ( $i \in \{1, \dots, N\}$ ) mobile robot can be described as

$$\begin{cases} \dot{x}_i = v_i \cos(\theta_i) \\ \dot{y}_i = v_i \sin(\theta_i) \\ \dot{\theta}_i = \omega_i, \end{cases} \quad (1)$$

and

$$\begin{cases} m_i \dot{v}_i = f_i^v(v_i, \omega_i) + \frac{r_i}{2} \tau_i^v + d_i^v \\ I_i \dot{\omega}_i = f_i^\omega(v_i, \omega_i) + \frac{r_i}{2R_i} \tau_i^\omega + d_i^\omega \end{cases} \quad (2)$$

where  $p_i = [x_i, y_i]^T$  is the position of the  $i$ th mobile robot in the global coordinate frame,  $\theta_i$  is the heading angle,  $v_i$  and  $\omega_i$  are the linear and angular velocities defined in the body-fixed coordinate frame,  $m_i$  and  $I_i$  are the inertia parameters,  $f_i^v$  and  $f_i^\omega$  are the unknown Coriolis and damping terms,  $d_i^v$  and  $d_i^\omega$  are the external disturbances,  $\tau_i^v$  and  $\tau_i^\omega$  are the control torques,  $r_i$  is the radius of the wheel, and  $2R_i$  is the width of the  $i$ th robot.

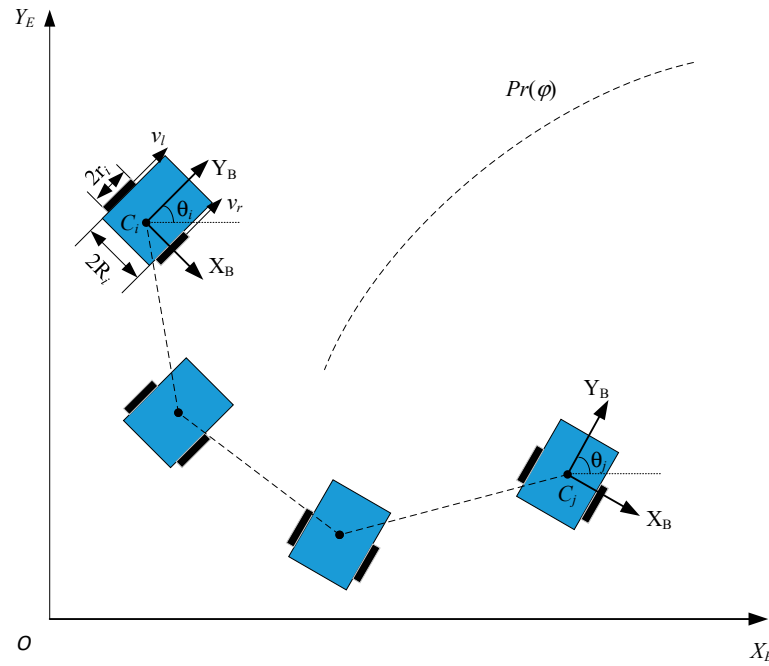


Figure 1. Formation model.

In the formation control problem, the mobile robots are guided by a virtual leader moving along the parameterized path  $p_r(\varphi) = [x_r(\varphi), y_r(\varphi)]^T$ . Here, the scalar variable  $\varphi$  is the time-dependent parameter of the parameterized path  $p_r(\varphi)$ . It is used to plan the desired path of the virtual leader. The mobile robots labeled as  $n_1, \dots, n_N$  move to follow the desired relative position and orientation. The following assumption is needed for the parameterized path:

**Assumption 2.** The parameterized path  $p_r(\varphi)$  and its derivative  $\partial p_r(\varphi) / \partial \varphi$  are bounded.

The control objective of this work is to develop an observer-based formation maneuvering protocol for mobile robots such that the following statements hold:

- (1) The mobile robots keep the desired formation described by

$$\lim_{t \rightarrow T} \|p_i - p_j - p_{ijd}\| < \epsilon_1, i = 1, \dots, N, j = r, 1, \dots, N \quad (3)$$

where  $\epsilon_1$  is a positive constant, and  $p_{ijd} \in \mathbf{R}^2$  is the desired geometry position between the  $i$ th robot and the  $j$ th robot.

- (2) The path parameter converges to a commanded speed  $v_s$  as follows:

$$|\dot{\varphi} - v_s| < \epsilon_2, \quad (4)$$

where  $v_s$  is the assigned speed of the path parameter, and  $\epsilon_2$  is a positive constant. The following lemma is introduced to achieve the above objectives:

**Lemma 1** [33]. Consider a general system  $\dot{x}(t) = f(x(t))$  with  $f(0) = 0$ , where  $f : U_1 \rightarrow R$  is the differential in an open neighborhood of the origin. Suppose there are positive constants  $c_1 > 0$ ,  $c_2 > 0$ ,  $\eta_1 \in (0, 1)$  and  $\eta_2$ , a differential Lyapunov function  $V(x)$  with the initial value  $V(x_0)$  such that  $\dot{V}(x) \leq -c_1 V^{\eta_1}(x)$  (or  $\dot{V}(x) \leq -c_1 V^{\eta_1}(x) - c_2 V(x)$ ); then, the trajectory of the system is finite-time convergent, where the convergence time is  $T \leq V(x_0)^{1-\eta_1} / c_1(1 - \eta_1)$  (or  $T \leq [c_2(1 - \eta_1)]^{-1} \ln[1 + c_1^{-1} c_2 V(x_0)^{1-\eta_1}]$ ).

### 3. Main Results

Figure 2 depicts the formation control scheme consisting of kinematic control and dynamic control. At the kinematic control level, the desired linear velocity  $v_{id}$ , heading angle  $\theta_{id}$ , and the path-parameter-updating law  $\omega_s$  are obtained such that control objectives (3) and (4) can be achieved. At the dynamic level, an anti-disturbance controller based on the estimated velocities and disturbances is developed to make  $v_i \rightarrow v_{id}$ ,  $\theta_i \rightarrow \theta_{id}$ ,  $\omega_i \rightarrow \omega_{id}$  in a finite time.

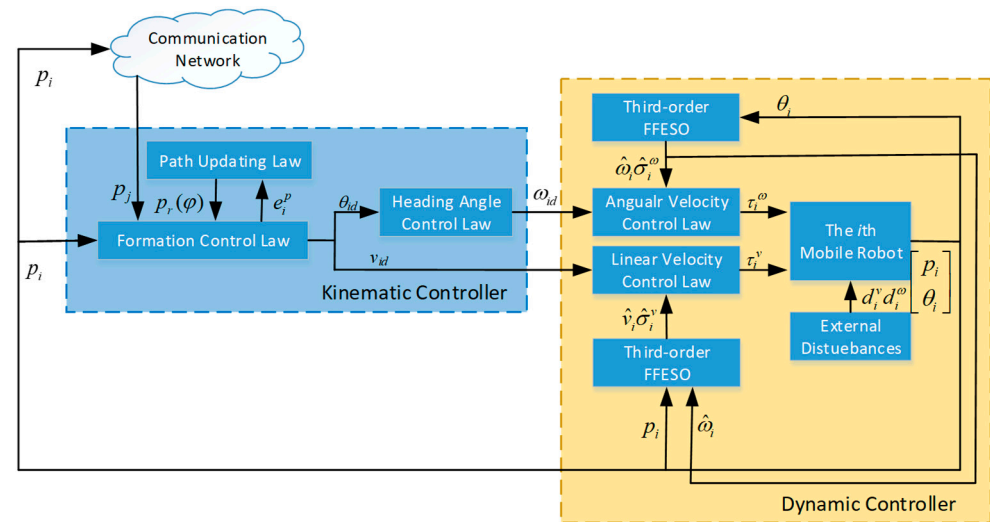


Figure 2. Control scheme.

#### 3.1. Observer Design

In this section, the design of an FFESO is discussed to estimate the unmeasured linear velocity, angular velocity, and total disturbances containing external disturbances and uncertainties.

Dynamics (2) of the mobile robots can be rewritten as

$$\dot{v}_i = a_1 \tau_i^v + \sigma_i^v, \tag{5}$$

and

$$\begin{cases} \dot{\theta}_i = w_i \\ \dot{\omega}_i = a_2 \tau_i^\omega + \sigma_i^\omega \end{cases} \tag{6}$$

where  $a_1 = \frac{r_i}{2m_i}$ ,  $\sigma_i^v = \frac{1}{m_i}(f_i^v(v_i, \omega_i) + d_i^v)$ , and  $a_2 = \frac{r_i}{2I_i R_i}$ ,  $\sigma_i^\omega = \frac{1}{I_i}(f_i^\omega(v_i, \omega_i) + d_i^\omega)$ . To facilitate the FFESO design, the following assumption is needed:

**Assumption 3.** There exist positive constants  $\bar{\sigma}_1$  and  $\bar{\sigma}_2$  such that  $\|\dot{\sigma}_i^v\| \leq \bar{\sigma}_1$  and  $\|\dot{\sigma}_i^\omega\| \leq \bar{\sigma}_2$ , respectively.

It is reasonable to assume that the derivative of the velocity-related variables  $\sigma_i^v$  and  $\sigma_i^\omega$  are bounded due to the limited energy of the external disturbances and velocities of practical mechanical systems.

Based on the abovementioned assumption, a finite-time observer is developed to estimate the unmeasured angular velocities and disturbances.

- (1) The following FFTESO is developed to estimate the unmeasured angular velocity  $\omega_i$  and the unknown signal  $\sigma_i^\omega$  based on the measured output information  $\theta_i$ .

$$\begin{cases} \dot{\hat{\theta}}_i = -b_{i1}(\text{sig}^\alpha(\hat{\theta}_i - \theta_i) + (\hat{\theta}_i - \theta_i)) + \hat{\omega}_i \\ \dot{\hat{\omega}}_i = -b_{i2}(\text{sig}^{2\alpha-1}(\hat{\theta}_i - \theta_i) + 2\text{sig}^\alpha(\hat{\theta}_i - \theta_i)) + \hat{\sigma}_i^\omega + a_2\tau_i^\omega \\ \dot{\hat{\sigma}}_i^\omega = -b_{i3}(\text{sig}^{2\alpha-1}(\hat{\theta}_i - \theta_i) + 2\text{sig}^\alpha(\hat{\theta}_i - \theta_i) + (\hat{\theta}_i - \theta_i)) \end{cases} \quad (7)$$

where  $\hat{\theta}_i$ ,  $\hat{\omega}_i$ , and  $\hat{\sigma}_i^\omega$  are the estimates of  $\theta_i$ ,  $\omega_i$ , and  $\sigma_i^\omega$ ; the parameters  $b_{i1}, b_{i2}, b_{i3} > 0$  are the control gains to be designed, and  $\alpha$  is a positive constant satisfying  $\frac{1}{2} < \alpha < 1$ .

Using (6) and (7), the estimation error system is given as follows:

$$\begin{cases} \dot{\tilde{\theta}}_i = -b_{i1}(\text{sig}^\alpha(\tilde{\theta}) + \tilde{\theta}) + \tilde{\omega}_i \\ \dot{\tilde{\omega}}_i = -b_{i2}(\text{sig}^{2\alpha-1}(\tilde{\theta}) + 2\text{sig}^\alpha(\tilde{\theta}) + \tilde{\theta}) + \tilde{\sigma}_i^\omega \\ \dot{\tilde{\sigma}}_i^\omega = -b_{i3}(\text{sig}^{2\alpha-1}(\tilde{\theta}) + 2\text{sig}^\alpha(\tilde{\theta}) + \tilde{\theta}) - \dot{\sigma}_i^\omega \end{cases} \quad (8)$$

where  $\tilde{\theta}_i = \hat{\theta}_i - \theta_i$ ,  $\tilde{\omega}_i = \hat{\omega}_i - \omega_i$ , and  $\tilde{\sigma}_i^\omega = \hat{\sigma}_i^\omega - \sigma_i^\omega$  are the estimation errors.

Then, the stability analysis of the estimation error system (8) is presented in the following theorem:

**Theorem 1.** *Considering the estimation error system (8) and Assumption 3, the estimation errors are finite-time uniformly ultimately bounded as stable if the observer gains  $b_{i1}, b_{i2}, b_{i3}$  and satisfies*

$$b_{i1}b_{i2} - b_{i3} > 0.$$

**Proof.** Choose the Lyapunov function candidate as follows:

$$V_1 = \sum_{i=1}^N \varepsilon_i^T P_i \varepsilon_i, \quad (9)$$

where  $\varepsilon_i = [\text{sig}^\alpha(\tilde{\theta}_i) + \tilde{\theta}_i, \tilde{\omega}_i, \tilde{\sigma}_i^\omega]^T$ , and  $P_i$  is a positive definite matrix.

Taking the time derivative  $\varepsilon_i$ , one has

$$\begin{aligned} \dot{\varepsilon}_i &= \begin{bmatrix} \alpha|\tilde{\theta}_i|^{\alpha-1}\dot{\tilde{\theta}}_i + \dot{\tilde{\theta}}_i \\ \dot{\tilde{\omega}}_i \\ \dot{\tilde{\sigma}}_i^\omega \end{bmatrix} \\ &= \begin{bmatrix} (\alpha|\tilde{\theta}_i|^{\alpha-1} + 1)(-b_{i1}(\text{sig}^\alpha(\tilde{\theta}_i) + \tilde{\theta}_i) + \tilde{\omega}_i) \\ -b_{i2}(\text{sig}^{2\alpha-1}(\tilde{\theta}) + 2\text{sig}^\alpha(\tilde{\theta}) + \tilde{\theta}) + \tilde{\sigma}_i^\omega \\ -b_{i3}(\text{sig}^{2\alpha-1}(\tilde{\theta}_i) + 2\text{sig}^\alpha(\tilde{\theta}_i) + \tilde{\theta}_i) - \dot{\sigma}_i^\omega \end{bmatrix} \\ &= \begin{bmatrix} \alpha|\tilde{\theta}_i|^{\alpha-1}(-b_{i1}(\text{sig}^\alpha(\tilde{\theta}_i) + \tilde{\theta}_i) + \tilde{\omega}_i) \\ -b_{i2}(\text{sig}^{2\alpha-1}(\tilde{\theta}_i) + \text{sig}^\alpha(\tilde{\theta}_i)) \\ -b_{i3}(\text{sig}^{2\alpha-1}(\tilde{\theta}_i) + \text{sig}^\alpha(\tilde{\theta}_i)) \end{bmatrix} \\ &+ \begin{bmatrix} -b_{i1}(\text{sig}^\alpha(\tilde{\theta}_i) + \tilde{\theta}_i) + \tilde{\omega}_i \\ -b_{i2}(\text{sig}^\alpha(\tilde{\theta}_i) + \tilde{\theta}_i) + \tilde{\sigma}_i^\omega \\ -b_{i3}(\text{sig}^\alpha(\tilde{\theta}_i) + \tilde{\theta}_i) \end{bmatrix} + \begin{bmatrix} 0 \\ 0 \\ -\dot{\sigma}_i^\omega \end{bmatrix} \\ &= \text{diag}(|\tilde{\theta}_i|^{\alpha-1}, |\tilde{\theta}_i|^{\alpha-1}, |\tilde{\theta}_i|^{\alpha-1})A_{i1}\varepsilon_i + A_{i2}\varepsilon_i + F_i \end{aligned} \quad (10)$$

where

$$A_{i1} = \begin{bmatrix} -\alpha b_{i1} & \alpha & 0 \\ -b_{i2} & 0 & 0 \\ -b_{i3} & 0 & 0 \end{bmatrix},$$

$$A_{i2} = \begin{bmatrix} -b_{i1} & 1 & 0 \\ -b_{i2} & 0 & 1 \\ -b_{i3} & 0 & 0 \end{bmatrix}$$

and  $F_i = [0, 0, -\dot{\sigma}_i^\omega]^T$ . The characteristic equation of matrix  $A_{i1}$  is  $\lambda^3 + \alpha b_{i1} \lambda^2 + \alpha b_{i2} \lambda$ , where  $\lambda$  is the eigenvalue of the above characteristic equation. The Hurwitz matrix of the characteristic equation is

$$\begin{bmatrix} \alpha b_{i2} & 0 & 0 \\ 1 & \alpha b_{i1} & \alpha b_{i2} \\ 0 & 0 & 1 \end{bmatrix}.$$

Based on the Routh–Hurwitz criterion, if the observer gains are selected to satisfy  $b_{i1} > 0, b_{i2} > 0, b_{i3} > 0$ , the characteristic equation is Hurwitz, which implies that matrix  $A_{i1}$  is Hurwitz. Similarly, matrix  $A_{i2}$  is Hurwitz if the observer gains are selected to satisfy (1)  $b_{i1} > 0, b_{i2} > 0, b_{i3} > 0$  and (2)  $b_{i1} b_{i2} - b_{i3} > 0$ . Therefore, there exist symmetric and positive-definite matrices  $P_i, Q_{i1}$  and  $Q_{i2}$  such that  $A_{i1}^T P_i + P_i A_{i1} = -Q_{i1}$  and  $A_{i2}^T P_i + P_i A_{i2} = -Q_{i2}$ .

Taking the time derivative  $V_1$ , one has

$$\begin{aligned} \dot{V}_1 &= \sum_{i=1}^N (\dot{\varepsilon}_i^T P_i \varepsilon_i + \varepsilon_i^T P_i \dot{\varepsilon}_i) \\ &= \sum_{i=1}^N (\varepsilon_i^T \text{diag}(|\tilde{\theta}_i|^{\alpha-1}, |\tilde{\theta}_i|^{\alpha-1}, |\tilde{\theta}_i|^{\alpha-1}) (A_{i1}^T P_i + P_i A_{i1}) \varepsilon_i \\ &\quad + \varepsilon_i^T (A_{i2}^T P_i + P_i A_{i2}) \varepsilon_i + 2\varepsilon_i^T P_i F_i) \\ &\leq \sum_{i=1}^N (-|\tilde{\theta}_i|^{\alpha-1} \lambda_{\min}(Q_{i1}) \|\varepsilon_i\|^2 - \lambda_{\min}(Q_{i2}) \|\varepsilon_i\|^2 + 2\|\varepsilon_i\| \|P_i\| \|F_i\|) \end{aligned} \tag{11}$$

Considering  $|\tilde{\theta}_i| \leq \|\varepsilon_i\|^{\frac{1}{\alpha}}$  and Assumption 3, we have

$$\begin{aligned} \dot{V}_1 &\leq -\sum_{i=1}^N \lambda_{\min}(Q_{i1}) \|\varepsilon_i\|^{3-\frac{1}{\alpha}} - \sum_{i=1}^N \lambda_{\min}(Q_{i2}) \|\varepsilon_i\|^2 + 2\sum_{i=1}^N \bar{\sigma}_2 \|\varepsilon_i\| \|P_i\| \\ &\leq -\lambda_1 \sum_{i=1}^N \|\varepsilon_i\|^{3-\frac{1}{\alpha}} - \lambda_2 \sum_{i=1}^N \|\varepsilon_i\|^2 + 2\bar{\sigma}_2 \|P_i\| \sum_{i=1}^N \|\varepsilon_i\| \\ &\leq -\mu_1 V_1^{\frac{3}{2}-\frac{1}{2\alpha}} - \mu_2 V_1 + \mu_3 V_1^{\frac{1}{2}} \leq -(\mu_1 - \bar{\iota}_1) V_1^{\frac{3}{2}-\frac{1}{2\alpha}} \\ &\quad - (\mu_2 - \bar{\iota}_2) V_1 - V_1^{\frac{1}{2}} [\bar{\iota}_1 V_1^{1-\frac{1}{2\alpha}} + \bar{\iota}_2 V_1^{\frac{1}{2}} - \mu_3] \end{aligned} \tag{12}$$

where  $\underline{\lambda}_1 = \min_{i=1, \dots, N} \{\lambda_{\min}(Q_{i1})\}, \underline{\lambda}_2 = \min_{i=1, \dots, N} \{\lambda_{\min}(Q_{i2})\}, \underline{\lambda}_3 = \min_{i=1, \dots, N} \{\lambda_{\min}(P_i)\},$   
 $\bar{\lambda}_4 = \max_{i=1, \dots, N} \{\lambda_{\max}(P_i)\}, \mu_1 = \frac{\underline{\lambda}_1}{(\bar{\lambda}_4)^{\frac{3}{2}-\frac{1}{2\alpha}}}, \mu_2 = \frac{\underline{\lambda}_2}{\underline{\lambda}_4}, \mu_3 = \frac{2\bar{\sigma}_2 \bar{\lambda}_4}{\underline{\lambda}_3}.$

From (12), we have  $\dot{V}_1 \leq -(\mu_1 - \bar{\iota}_1) V_1^{\frac{3}{2}-\frac{1}{2\alpha}} - (\mu_2 - \bar{\iota}_2) V_1$  if  $\bar{\iota}_1 V_1^{1-\frac{1}{2\alpha}} + \bar{\iota}_2 V_1^{\frac{1}{2}} - \mu_3 \geq 0$ . According to Lemma 1, the error vector  $\varepsilon_i$  converges to the following stable region in a finite time:

$$\Theta_1 = \{\varepsilon_i : \bar{\iota}_1 V_1^{1-\frac{1}{2\alpha}} + \bar{\iota}_2 V_1^{\frac{1}{2}} < \mu_3\} \tag{13}$$

where  $\bar{\iota}_1 \in (0, \mu_1)$  and  $\bar{\iota}_2 \in (0, \mu_2)$ .

The convergence time is

$$T_1 \leq \frac{2}{(\mu_2 - \bar{\iota}_2)(1 - \alpha)} \ln\left(\frac{(\mu_2 - \bar{\iota}_2) V_1^{\frac{1}{2\alpha}-\frac{1}{2}}}{\mu_1 - \bar{\iota}_1} + 1\right), \tag{14}$$

which completes the proof.  $\square$

1. The FFTESO for the estimation of unmeasured linear velocity is given as follows for  $v_i$  and the unknown signal  $\sigma_i^v$ :

$$\begin{cases} \dot{\hat{q}}_i = -\gamma_{i1}(\text{sig}^\alpha(\hat{q}_i - q_i) + (\hat{q}_i - q_i)) + \hat{v}_i + \hat{\omega}(-x_i \sin(\theta_i) + y_i \cos(\theta_i)) \\ \dot{\hat{v}}_i = -\gamma_{i2}(\text{sig}^{2\alpha-1}(\hat{q}_i - q_i) + 2\text{sig}^\alpha(\hat{q}_i - q_i) + (\hat{q}_i - q_i)) + \hat{\sigma}_i^v + a_1 \tau_i^v \\ \dot{\hat{\sigma}}_i^v = -\gamma_{i3}(\text{sig}^{2\alpha-1}(\hat{q}_i - q_i) + 2\text{sig}^\alpha(\hat{q}_i - q_i) + (\hat{q}_i - q_i)) \end{cases} \quad (15)$$

where  $q_i = x_i \cos(\theta_i) + y_i \sin(\theta_i)$ ;  $\hat{q}_i$ ,  $\hat{v}_i$  and  $\hat{\sigma}_i^v$  are the estimates of  $q_i$ ,  $v_i$  and  $\sigma_i^v$ , respectively. The parameters  $\gamma_{i1}, \gamma_{i2}, \gamma_{i3} > 0$  are the gains to be designed, and  $\alpha$  is a positive constant satisfying  $\frac{1}{2} < \alpha < 1$ .

The estimation error system is given as follows:

$$\begin{cases} \dot{\tilde{q}}_i = -\gamma_{i1}(\text{sig}^\alpha(\tilde{q}_i) + \tilde{q}_i) + \tilde{v}_i + \tilde{\omega}_i(-x_i \sin(\theta_i) + y_i \cos(\theta_i)) \\ \dot{\tilde{v}}_i = -\gamma_{i2}(\text{sig}^{2\alpha-1}(\tilde{q}_i) + 2\text{sig}^\alpha(\tilde{q}_i) + \tilde{q}_i) + \tilde{\sigma}_i^v \\ \dot{\tilde{\sigma}}_i^v = -\gamma_{i3}(\text{sig}^{2\alpha-1}(\tilde{q}_i) + 2\text{sig}^\alpha(\tilde{q}_i) + \tilde{q}_i) - \dot{\sigma}_i^v \end{cases} \quad (16)$$

where  $\tilde{q}_i = \hat{q}_i - q_i$ ,  $\tilde{v}_i = \hat{v}_i - v_i$ , and  $\tilde{\sigma}_i^v = \hat{\sigma}_i^v - \sigma_i^v$  are the estimation errors.

The stability analysis of the estimation error system (16) is presented in the following theorem:

**Theorem 2.** *Considering the estimation error system (16) and Assumption 3, the estimation errors are finite-time uniformly ultimately bounded as stable if the observer gains  $\gamma_{i1}, \gamma_{i2}, \gamma_{i3}$  and satisfies  $\gamma_{i1}\gamma_{i2} - \gamma_{i3} > 0$ .*

**Proof.** After time  $T_1$ , the estimated angular velocity  $\hat{\omega}_i$  converges to  $\omega_i$ , and the error system (16) becomes

$$\begin{cases} \dot{\tilde{q}}_i = -\gamma_{i1}(\text{sig}^\alpha(\tilde{q}_i) + \tilde{q}_i) + \tilde{v}_i \\ \dot{\tilde{v}}_i = -\gamma_{i2}(\text{sig}^{2\alpha-1}(\tilde{q}_i) + 2\text{sig}^\alpha(\tilde{q}_i) + \tilde{q}_i) + \tilde{\sigma}_i^v \\ \dot{\tilde{\sigma}}_i^v = -\gamma_{i3}(\text{sig}^{2\alpha-1}(\tilde{q}_i) + 2\text{sig}^\alpha(\tilde{q}_i) + \tilde{q}_i) - \dot{\sigma}_i^v \end{cases} \quad (17)$$

which has the same form as the system in (8).

The following Lyapunov candidate function is chosen:

$$V_2 = \sum_{i=1}^N \zeta_i^T P_i \zeta_i, \quad (18)$$

where  $\zeta_i = [\text{sig}^\alpha(\tilde{q}_i) + \tilde{q}_i, \tilde{v}_i, \tilde{\sigma}_i^v]^T$ , and  $P_i$  is a positive definite matrix.

Similar to the proof of Theorem 1, we have

$$\begin{aligned} \dot{V}_2 &\leq -l_1 V_2^{\frac{3}{2} - \frac{1}{2\alpha}} - l_2 V_2 + l_3 V_2^{\frac{1}{2}} \\ &\leq -(l_1 - l_1) V_2^{\frac{3}{2} - \frac{1}{2\alpha}} - (l_2 - l_2) V_2 - V_2^{\frac{1}{2}} [l_1 V_2^{1 - \frac{1}{2\alpha}} + l_2 V_2^{\frac{1}{2}} - l_3]. \end{aligned} \quad (19)$$

From (19), we have  $\dot{V}_2 \leq -(l_1 - l_1) V_2^{\frac{3}{2} - \frac{1}{2\alpha}} - (l_2 - l_2) V_2$  if  $l_1 V_2^{1 - \frac{1}{2\alpha}} + l_2 V_2^{\frac{1}{2}} - l_3 \geq 0$ . According to Lemma 1, the error vector  $\zeta_i$  converges to the following stable region:

$$\Theta_2 = \{\zeta_i : l_1 V_2^{1 - \frac{1}{2\alpha}} + l_2 V_2^{\frac{1}{2}} < l_3\} \quad (20)$$

where  $l_1 \in (0, l_1)$  and  $l_2 \in (0, l_2)$ .

The convergence time is

$$T_2 \leq T_1 + \frac{2}{(l_2 - l_1)(1 - \alpha)} \ln\left(\frac{(l_2 - l_1)V_2^{\frac{1}{2\alpha} - \frac{1}{2}}}{l_1 - l_1} + 1\right), \tag{21}$$

which completes the proof.  $\square$

**Remark 1.** Compared with the finite-time extended state observer proposed in [26], which only contains the term  $\text{sig}^\alpha(\cdot)$ , the combination of the term  $\text{sig}^\alpha(\tilde{\theta}_i)$  (or  $\text{sig}^\alpha(\tilde{q}_i)$ ) and the linear term  $\tilde{\theta}_i$  (or  $\tilde{q}_i$ ) in the proposed fast finite-time extended state observers (7) (or (15)) accelerate the convergence speed. This is because when the estimation error satisfies  $\tilde{\theta}_i \geq 1$  and  $\tilde{q}_i \geq 1$ ,  $\tilde{\theta}_i$  and  $\tilde{q}_i$  play the major role instead of the terms  $\text{sig}^\alpha(\tilde{\theta}_i)$  and  $\text{sig}^\alpha(\tilde{q}_i)$ , which accelerate the convergence speed to the regions  $\tilde{\theta}_i < 1$  and  $\tilde{q}_i < 1$ . Once the estimation error converges to the regions  $\tilde{\theta}_i < 1$  and  $\tilde{q}_i < 1$ , the terms  $\text{sig}^\alpha(\tilde{\theta}_i)$  and  $\text{sig}^\alpha(\tilde{q}_i)$  play the major role instead.

### 3.2. Kinematic Controller Design

In this section, the double closed-loop control strategy is applied for the kinematic controller design. In the outer loop of multiple mobile robots, a velocity control law is designed for the formation control. In the inner loop, an attitude control law is designed for the heading angle tracking control.

The distributed formation error is defined as follows:

$$e_i^p = \sum_{j=1}^N a_{ij}(p_i - p_j - p_{ijd}) + a_{i0}(p_i - p_r - p_{id}), \tag{22}$$

where  $p_{ijd} = p_{id} - p_{jd}$ , and  $e_i^p$  is the distributed formation error expressed in the global coordinate frame.

Differentiating  $e_i^p$  yields

$$\begin{aligned} \dot{e}_i^p &= s_i \dot{p}_i - \sum_{j=1}^N a_{ij} \dot{p}_j - a_{i0} \frac{\partial p_r}{\partial \varphi} \dot{\varphi} \\ &= s_i \vartheta_{id} + s_i \delta_{ie} - s_i \zeta_{ie} - \sum_{j=1}^N a_{ij} \dot{p}_j - a_{i0} \frac{\partial p_r}{\partial \varphi} (v_s - \omega_s), \end{aligned} \tag{23}$$

where  $s_i = \sum_{j=1}^N a_{ij} + a_{i0}$ ,  $\delta_{ie} = \hat{\theta}_i - \vartheta_{id}$ ,  $\zeta_{ie} = \hat{\theta}_i - \vartheta_i$ ,  $\vartheta_{id} = \dot{p}_{id} = \begin{bmatrix} v_{id} \cos(\theta_{id}) \\ v_{id} \sin(\theta_{id}) \end{bmatrix}$ ,  $\hat{\theta}_i = \hat{v}_i \begin{bmatrix} \cos(\hat{\theta}_i) \\ \sin(\hat{\theta}_i) \end{bmatrix}$ ,  $\vartheta_i = v_i \begin{bmatrix} \cos(\theta_i) \\ \sin(\theta_i) \end{bmatrix}$ ,  $\dot{\varphi} = v_s - \omega_s$ .

The desired guidance vector is designed to stabilize error dynamics (23) as follows:

$$\begin{aligned} \vartheta_{id} &= \begin{bmatrix} \vartheta_{idx} \\ \vartheta_{idy} \end{bmatrix} = v_{id} \begin{bmatrix} \cos(\theta_{id}) \\ \sin(\theta_{id}) \end{bmatrix} \\ &= \frac{1}{s_i} (-k_i^p \text{sig}^{\beta_i^p}(e_i^p) + \sum_{j=1}^N a_{ij} \dot{p}_j \begin{bmatrix} \cos(\hat{\theta}_j) \\ \sin(\hat{\theta}_j) \end{bmatrix} + a_{i0} \frac{\partial p_r}{\partial \varphi} v_s), \end{aligned} \tag{24}$$

where  $k_i^p$  is a positive control gain to be designed,  $\beta_i^p$  is a positive constant satisfying  $0 < \beta_i^p < 1$ , and  $v_{id}$ ,  $\theta_{id}$  are the desired linear velocity and heading angle of the mobile robot, respectively.

According to (24), the desired linear velocity  $v_{id}$  and the desired heading angle  $\theta_{id}$  can be designed as follows:

$$\theta_{id} = \text{atan2}(\vartheta_{idy}, \vartheta_{idx}) + 2k\pi, \tag{25}$$

$$v_{id} = \|\vartheta_{id}\|. \tag{26}$$

To make the derivative of the path parameter converge to a commanded speed, a path-updating law is designed as follows:

$$\dot{\omega}_s = -\rho_1(\text{sig}^{\beta^s}(\omega_s) + \rho_2 \sum_{i=1}^N a_{i0} \left(\frac{\partial p_r}{\partial \varphi}\right)^T e_i^p), \tag{27}$$

where  $\rho_1$  and  $\rho_2$  are the positive control gains to be designed, and  $\beta^s$  is a positive constant satisfying  $0 < \beta^s < 1$ .

### 3.3. FFTESO-Based Dynamic Controller Design

To realize the tracking control of the estimated linear velocity  $\hat{v}_i$  to the desired linear velocity  $v_{id}$ , the tracking error  $e_i^v$  is defined as follows:

$$e_i^v = \hat{v}_i - v_{id}. \tag{28}$$

Differentiating  $e_i^v$  yields

$$\dot{e}_i^v = -\gamma_{i2}(\text{sig}^{2\alpha-1}(\tilde{q}_i) + 2\text{sig}^\alpha(\tilde{q}_i) + \tilde{q}_i) + \hat{\sigma}_i^v + a_1 \tau_i^v - \dot{v}_{id}. \tag{29}$$

To stabilize the tracking error  $e_i^v$ , the following control law is designed:

$$\tau_i^v = \frac{1}{a_1}(-k_i^v \text{sig}^{\beta_i^v}(e_i^v) + \gamma_{i2}(\text{sig}^{2\alpha-1}(\tilde{q}_i) + 2\text{sig}^\alpha(\tilde{q}_i) + \tilde{q}_i) - \hat{\sigma}_i^v + \dot{v}_{id}), \tag{30}$$

To realize the tracking control of the heading angle  $\hat{\theta}_i$  to the desired heading angle  $\theta_{id}$  obtained in (25), the following angle tracking error is defined:

$$e_i^\theta = \hat{\theta}_i - \theta_{id}. \tag{31}$$

Differentiating  $e_i^\theta$  yields

$$\dot{e}_i^\theta = -b_{i1}(\text{sig}^\alpha(\tilde{\theta}_i) + \tilde{\theta}_i) + \omega_{id} + e_i^\omega - \dot{\theta}_{id}, \tag{32}$$

where  $e_i^\omega = \hat{\omega}_i - \omega_{id}$  is the tracking error of the angular velocity.

In order to stabilize the tracking error  $e_i^\theta$ , the following attitude control law is designed:

$$\omega_{id} = -k_i^\theta \text{sig}^{\beta_i^\theta}(e_i^\theta) + b_{i1}(\text{sig}^\alpha(\tilde{\theta}_i) + \tilde{\theta}_i) + \dot{\theta}_{id}, \tag{33}$$

where  $k_i^\theta \in \mathbf{R}$  is the control gain to be designed, and  $\beta_i^\theta$  is a positive constant satisfying  $0 < \beta_i^\theta < 1$ .

where  $k_i^v \in \mathbf{R}$  is the control gain to be designed, and  $\beta_i^v$  is a positive constant satisfying  $0 < \beta_i^v < 1$ .

To realize the tracking control of the estimated angular velocity  $\hat{\omega}_i$  to the desired angular velocity  $\omega_{id}$ , the tracking error  $e_i^\omega$  is defined in (29). Differentiating  $e_i^\omega$  yields

$$\dot{e}_i^\omega = -b_{i2}(2\text{sig}^\alpha(\tilde{\theta}_i) + 2\tilde{\theta}_i) + \hat{\sigma}_i^\omega + a_2 \tau_i^\omega - \dot{\omega}_{id}. \tag{34}$$

To stabilize the tracking error  $e_i^\omega$ , the following control law is designed:

$$\tau_i^\omega = \frac{1}{a_2}(-k_i^\omega \text{sig}^{\beta_i^\omega}(e_i^\omega) + b_{i2}(\text{sig}^{2\alpha-1}(\tilde{\theta}_i) + 2\text{sig}^\alpha(\tilde{\theta}_i) + 2\tilde{\theta}_i) - \hat{\sigma}_i^\omega + \dot{\omega}_{id} - e_i^\omega), \tag{35}$$

where  $k_i^\omega \in \mathbf{R}$  is the control gain to be designed, and  $\beta_i^\omega$  is a positive constant satisfying  $0 < \beta_i^\omega < 1$ .

**Remark 2.** It can be observed from that (30), (33), and (35) that the time derivative  $\dot{\theta}_{id}$ ,  $\dot{\omega}_{id}$ , and  $\dot{v}_{id}$  are required in the controller design. In engineering, the noise will be amplified if we take the first derivative of signals  $\theta_{id}$ ,  $\omega_{id}$ , and  $v_{id}$  directly. Therefore, the second-order finite-time tracking differentiator proposed in [34] is employed to obtain the estimation of the first derivative of the signals and suppress noise.

### 3.4. Stability Analysis

Substituting (24) into (23) and using (27), the kinematic error system is given as follows:

$$\begin{cases} \dot{e}_i^p = -k_i^p \text{sig}^{\beta_i^p}(e_i^p) + s_i \delta_{ie} - s_i \zeta_{ie} + \sum_{j=1}^N a_{ij} \zeta_{je} + a_{i0} \frac{\partial p_r}{\partial \varphi} \omega_s \\ \dot{\omega}_s = -\rho_1 (\text{sig}^{\beta_s}(\omega_s) + \rho_2 \sum_{i=1}^N a_{i0} (\frac{\partial p_r}{\partial \varphi})^T e_i^p). \end{cases} \quad (36)$$

Substituting (30), (33), and (35) into (29), (32), and (34), the dynamic error system is given as follows:

$$\begin{cases} \dot{e}_i^v = -k_i^v \text{sig}^{\beta_i^v}(e_i^v) \\ \dot{e}_i^\theta = -k_i^\theta \text{sig}^{\beta_i^\theta}(e_i^\theta) + e_i^\omega \\ \dot{e}_i^\omega = -k_i^\omega \text{sig}^{\beta_i^\omega}(e_i^\omega) - e_i^\theta \end{cases} \quad (37)$$

The stability analysis of the closed-loop systems (36) and (37) are given in the following two theorems:

**Theorem 3.** Consider a network of nonholonomic mobile robots with dynamics (1) and (2) with the kinematic control laws (25), (26), and the path-updating law (27). If Assumptions 1–3 are satisfied, the subsystem (36) is finite-time uniformly ultimately bounded stable.

**Proof.** Choose the Lyapunov function candidate as follows:

$$V_3 = \frac{1}{2} \sum_{i=1}^N (e_i^p)^T e_i^p + \frac{1}{\rho_1 \rho_2} \omega_s^2. \quad (38)$$

Taking the time derivative of  $V_3$  yields

$$\begin{aligned} \dot{V}_3 &= \sum_{i=1}^N [(e_i^p)^T [-k_i^p \text{sig}^{\beta_i^p}(e_i^p) + s_i \delta_{ie} - s_i \zeta_{ie} + \sum_{j=1}^N a_{ij} \zeta_{je} - a_{i0} \frac{\partial p_r}{\partial \varphi} \omega_s] \\ &+ \frac{1}{\rho_1 \rho_2} \omega_s [-\rho_1 (\text{sig}^{\beta_s}(\omega_s) + \rho_2 \sum_{i=1}^N a_{i0} (\frac{\partial p_r}{\partial \varphi})^T e_i^p)] \\ &= \sum_{i=1}^N [-k_i^p (e_i^p)^T \text{sig}^{\beta_i^p}(e_i^p)] - \frac{1}{\rho_2} |\omega_s|^{\beta_s+1} \\ &+ \sum_{i=1}^N [(e_i^p)^T (s_i \delta_{ie} - s_i \zeta_{ie} + \sum_{j=1}^N a_{ij} \zeta_{je})]. \end{aligned} \quad (39)$$

Denote  $E_1 = [(e_1^p)^T, \dots, (e_N^p)^T, \omega_s]^T$ . According to inequality  $\sum_{i=1}^N (z_i)^p \geq N^{1-p} (\sum_{i=1}^N z_i)^p$  with the positive real numbers  $z_1, \dots, z_N > 0$  and  $p > 1$ , we have

$$\begin{aligned} \dot{V}_3 &\leq -k_1^* (2N + 1)^{-\beta_1^*} [\sum_{i=1}^N \|e_i^p\|_1 + |\omega_s|]^{1+\beta_1^*} \\ &+ \sum_{i=1}^N \|e_i^p\| (s_i \|\delta_{ie}\| + s_i \|\zeta_{ie}\| + \sum_{j=1}^N a_{ij} \|\zeta_{je}\|) \\ &\leq -\kappa_1 \|E_1\|^{\beta_1^*+1} + \|Y_e\| \|E_1\| \end{aligned} \quad (40)$$

where  $\|Y_e\| = \max_{1 \leq i \leq N} \{s_i \|\delta_{ie}\| + s_i \|\zeta_{ie}\| + \sum_{j=1}^N a_{ij} \|\zeta_{je}\|\}$ ,  $k_1^* = \min_{i=1, \dots, N} \{k_i^p, \frac{1}{\rho_2}\}$ ,  $\beta_1^* = \min_{i=1, \dots, N} \{\beta_i^p, \beta_i^s\}$ , and  $\kappa_1 = k_1^*(2N + 1)^{-\beta_1^*}$ . The errors  $\|\zeta_{ie}\|$ , and  $\|\zeta_{je}\|$  are bounded since the estimation errors are finite-time uniformly ultimately bounded. We assume that  $\|\delta_{ie}\|$  is bounded, which will be proved in the next theorem. Then, there exists a positive constant  $Y^*$  such that  $\|Y_e\| \leq Y^*$ . One has

$$\dot{V}_3 \leq -(\kappa_1 - \frac{\|Y^*\|}{\|E_1\|^{\beta_1^*}}) \|E_1\|^{\beta_1^*+1} \tag{41}$$

According to Lemma 1,  $\|E_1\| \leq \frac{\|Y^*\|}{\kappa_1}$  can be reached in a finite time. The convergence time is

$$T_4 \leq \frac{V_4^{\frac{1-\beta_1^*}{2}}}{\kappa_1(1-\beta_1^*)}. \tag{42}$$

□

**Theorem 4.** Consider a network of nonholonomic mobile robots with dynamics (1) and (2) with the dynamic control laws (30), (33), and (35). If Assumptions 1–3 are satisfied, subsystem (37) is finite-time stable.

**Proof.** Choose the Lyapunov function candidate as follows:

$$V_4 = \frac{1}{2} \sum_{i=1}^N [(e_i^v)^2 + (e_i^\theta)^2 + (e_i^\omega)^2] \tag{43}$$

Taking the time derivative of  $V_4$  yields

$$\begin{aligned} \dot{V}_4 &= \sum_{i=1}^N [e_i^v (-k_i^v \text{sig}^{\beta_i^v}(e_i^v)) + e_i^\theta [-k_i^\theta \text{sig}^{\beta_i^\theta}(e_i^\theta) + e_i^\omega] + e_i^\omega [-k_i^\omega \text{sig}^{\beta_i^\omega}(e_i^\omega) - e_i^\theta]] \\ &= \sum_{i=1}^N [-k_i^v |e_i^v|^{\beta_i^v+1} - k_i^\theta |e_i^\theta|^{\beta_i^\theta+1} - k_i^\omega |e_i^\omega|^{\beta_i^\omega+1}] \end{aligned} \tag{44}$$

Denote  $E_{i2} = [e_i^v, e_i^\theta, e_i^\omega]^T$ . According to inequality  $\sum_{i=1}^N (z_i)^p \geq N^{1-p} (\sum_{i=1}^N z_i)^p$  with the positive real numbers  $z_1, \dots, z_N > 0$  and  $p > 1$ , we have

$$\begin{aligned} \dot{V}_4 &\leq -\kappa_2^*(3N)^{-\beta_2^*} [\sum_{i=1}^N (|e_i^v| + |e_i^\theta| + |e_i^\omega|)]^{1+\beta_2^*} \\ &\leq -\kappa_2 \sum_{i=1}^N \|E_{i2}\|^{\beta_2^*+1} \end{aligned} \tag{45}$$

where  $k_2^* = \min_{i=1, \dots, N} \{k_i^v, k_i^\theta, k_i^\omega\}$ ,  $\beta_2^* = \min_{i=1, \dots, N} \{\beta_i^v, \beta_i^\theta, \beta_i^\omega\}$ , and  $\kappa_2 = k_2^*(3N)^{-\beta_2^*}$ . From (45), we have

$$\dot{V}_4 \leq -\kappa_4 V_4^{\frac{\beta_2^*+1}{2}}. \tag{46}$$

The convergence time is

$$T_5 \leq \frac{V_4^{\frac{1-\beta_2^*}{2}}}{\kappa_2(1-\beta_2^*)}, \tag{47}$$

According to Lemma 1, subsystem (37) is finite-time stable, implying that  $\lim_{t \rightarrow T_4} \hat{v}_i = v_{id}$ ,

$\lim_{t \rightarrow T_4} \hat{\theta}_i = \theta_{id}$ ,  $\lim_{t \rightarrow T_4} \hat{\omega}_i = \omega_{id}$ . Hence, the tracking error  $\|\delta_{ie}\|$  is bounded. □

In Theorems 1–4, the stability of the observer subsystem, the kinematic subsystem, and the dynamic subsystem is analyzed. Through the following theorem, the stability of the closed-loop cascade system is synthesized:

**Theorem 5.** Consider a network of nonholonomic mobile robots with dynamics (1) and (2) with FFTESOs (7) and (15), the kinematic control laws (25), (26), the path-updating law (27), and the dynamic control laws (30), (33), and (35). If Assumptions 1–3 are satisfied, the distributed formation control can be achieved, and the errors in the closed-loop systems (36) and (37) are finite-time uniformly ultimately bounded stable.

**Proof.** According to Theorems 3 and 4, the system cascaded by subsystems (36) and (37) is finite-time uniformly ultimately bounded stable. From Theorems 3, the error vector satisfies  $\|E_1\| \leq \frac{\|Y^*\|}{\kappa_1}$ , which means that there exist positive constants  $\epsilon_1$  and  $\epsilon_2$  such that (3) and (4) are satisfied, which completes the proof.  $\square$

**Remark 3.** A single-path-guided formation control scheme is proposed in this article, which makes multiple mobile robots keep the desired formation while tracking the parameterized path with a specified speed. Compared with the results in [7–13], where each mobile robot was assigned a desired parameterized path, the single-path-guided formation control scheme proposed in this article saves communication and computing resources.

#### 4. Simulation Results

In this section, the results of the conducted simulation studies are presented to demonstrate the effectiveness of the proposed formation control protocols. MATLAB R2014a/Simulink software was used for simulation purposes, and the ode45 (Dormand-Prince) solver was used for the differential calculations with a relative tolerance value of 0.001. The considered system consisted of four mobile robots and a virtual leader moving along a parameterized path. Only one robot was assumed to have the ability to access the information of the desired path. The information exchange among the mobile robots was directed, and the communication topology between the mobile robots is shown in Figure 3.

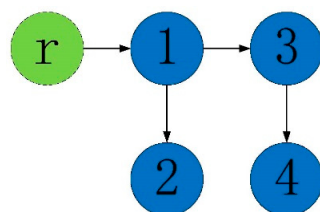


**Figure 3.** The communication topology of the NMRs.

The parameters of the mobile robots used in the simulations are the same as those in [35] and presented in Table 1. The initial conditions of the mobile robots were chosen as  $[x_1(0), y_1(0), \theta_1(0)]^T = [-1.3, 10.5, 0.2]^T$ ,  $[x_2(0), y_2(0), \theta_2(0)]^T = [-1.4, 10.5, 0.2]^T$ ,  $[x_3(0), y_3(0), \theta_3(0)]^T = [-1, 9, 0.2]^T$ ,  $[x_4(0), y_4(0), \theta_4(0)]^T = [-0.1, 5, 0.2]^T$ . The desired path was generated by  $p_r(\varphi) = [10 \sin(0.5\varphi), 10 \cos(0.5\varphi)]^T$ , with the commanded speed  $v_s = 0.5$ . The desired geometry position vectors were chosen as  $p_{1d} = [0, 0]^T$ ,  $p_{2d} = [-3, 0]^T$ ,  $p_{3d} = [0, -3]^T$ , and  $p_{4d} = [-3, -3]^T$ . The extended state observer gains were set as  $b_{i1} = 90$ ,  $b_{i2} = 2700$ ,  $b_{i3} = 27000$ ,  $\gamma_{i1} = 90$ ,  $\gamma_{i2} = 2700$ ,  $\gamma_{i3} = 27000$ , and  $\alpha = 0.95$ . The control gains of the path-updating law were set as  $\rho_1 = \rho_3 = 0.3$  and  $\beta^s = 0.5$ . The control gains were set as  $k_i^p = 15$ ,  $k_i^v = 15$ ,  $k_i^\theta = 5$ ,  $k_i^\omega = 10$ ,  $\beta_i^p = 0.95$ ,  $\beta_i^v = 0.95$ ,  $\beta_i^\theta = 0.95$ , and  $\beta_i^\omega = 0.95$ . To demonstrate the effectiveness of the proposed FFTESO-based formation control protocols, the bounded external disturbances were given as follows:

$$d_1(t) = \begin{bmatrix} 4 \cos(t) \\ 2 \sin(t) \end{bmatrix}$$

$$d_2(t) = \begin{bmatrix} 2 + 4 \sin(2t) \\ 2 \cos(2t) \end{bmatrix}$$

$$d_3(t) = \begin{bmatrix} -2 + 3 \sin(t) \\ -1 + 2 \cos(3t) \end{bmatrix}$$

$$d_4(t) = \begin{bmatrix} 2 + 3 \sin(4t) \\ 1 + 2 \cos(4t) \end{bmatrix}$$

**Table 1.** Parameters of the mobile robots.

Parameter	The <i>i</i> th Mobile Robot	Unit
$m_i$	0.365	Kg m <sup>2</sup>
$I_i$	0.3941	Kg m <sup>2</sup>
$r_i$	0.15	m
$R_i$	0.75	m

The comparisons between the different observers are shown in Figure 4. For clarity, we only show the comparison results of one mobile robot. The other mobile robots resulted in the same conclusions, because the applied observers were distributed. By employing the proposed FFTESO (7) and (15), the estimation errors of the unmeasured velocities  $v_i$  and  $\omega_i$  and the disturbance signals  $\sigma_i^v$  and  $\sigma_i^\omega$  are shown in Figure 4. To demonstrate the superiority of the proposed FFTESO, the comparisons with the linear extended state observer (LESO) proposed in [29] and the finite-time extended state observer (FTESO) proposed in [26] were made. The observer gains and initial conditions of the linear extended state observer in [29] and the finite-time extended state observer in [26] are the same as those in this article. It can be observed from Figure 4 that the settling time and estimation error of the proposed FFTESO is less than those under the methods proposed in [29] and [26]. The following performance indices were used to evaluate the performance of the proposed FFTESO: the integral of the absolute value of the error (IAE), the integral of the square error (ISE), the integral of the time multiplied by the absolute value of the error (ITAE), and the integral of the time multiplied by the square error (ITSE). The comparisons of the performance indices of the scheme are shown in Tables 2–5. Small performance index values represent good performance. It can be observed that the performance of the proposed FFTESO is better than that of the FFESO and LESO.

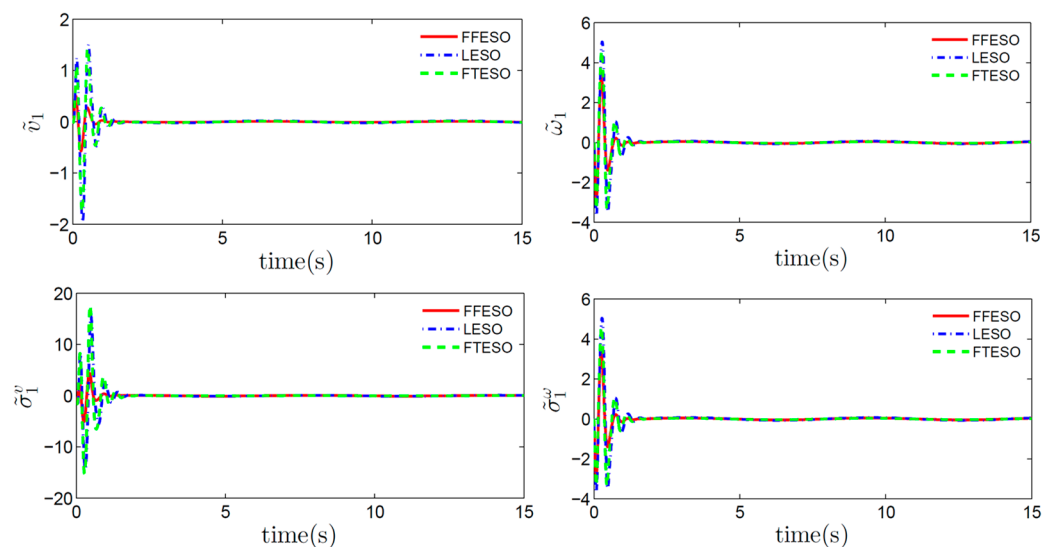


**Figure 4.** Comparison results of the proposed FFTESO, FTESO proposed in [26], and LESO proposed in [29].

**Table 2.** Comparison of performance indices of the estimated linear velocity.

Controller	Actual Value	Performance Indices			
	Estimation	IAE	ISE	ITAE	ITSE
LESO	$\tilde{v}_1 = \hat{v}_1 - v_1$	0.939	0.824	1.915	0.349
FTESO	$\tilde{v}_1 = \hat{v}_1 - v_1$	0.759	0.648	1.156	0.254
Proposed FFTESO	$\tilde{v}_1 = \hat{v}_1 - v_1$	0.244	0.063	0.596	0.020

**Table 3.** Comparison of performance indices of the estimated angular velocity.

Controller	Actual Value	Performance Indices			
	Estimation	IAE (10 <sup>-2</sup> )	ISE (10 <sup>-3</sup> )	ITAE	ITSE (10 <sup>-3</sup> )
LESO	$\tilde{\omega}_1 = \hat{\omega}_1 - \omega_1$	7.971	5.613	0.180	2.210
FTESO	$\tilde{\omega}_1 = \hat{\omega}_1 - \omega_1$	6.292	4.322	0.106	1.523
Proposed FFTESO	$\tilde{\omega}_1 = \hat{\omega}_1 - \omega_1$	2.312	0.553	0.058	0.168

**Table 4.** Comparison of performance indices of the estimated signals  $\sigma_1^v$ .

Controller	Actual Value	Performance Indices			
	Estimation	IAE	ISE	ITAE	ITSE
LESO	$\tilde{\sigma}_1^v = \hat{\sigma}_1^v - \sigma_1^v$	6.807	52.38	9.494	22.49
FTESO	$\tilde{\sigma}_1^v = \hat{\sigma}_1^v - \sigma_1^v$	6.993	61.49	6.899	25.369
Proposed FFTESO	$\tilde{\sigma}_1^v = \hat{\sigma}_1^v - \sigma_1^v$	2.255	4.882	5.824	1.893

**Table 5.** Comparison of performance indices of the estimated signals  $\sigma_1^\omega$ .

Controller	Actual Value	Performance Indices			
	Estimation	IAE	ISE	ITAE	ITSE
LESO	$\tilde{\sigma}_1^\omega = \hat{\sigma}_1^\omega - \sigma_1^\omega$	2.439	5.363	5.376	1.917
FTESO	$\tilde{\sigma}_1^\omega = \hat{\sigma}_1^\omega - \sigma_1^\omega$	1.979	4.366	3.461	1.394
Proposed FFTESO	$\tilde{\sigma}_1^\omega = \hat{\sigma}_1^\omega - \sigma_1^\omega$	1.398	2.044	3.183	0.592

Based on the proposed FFTESO, the output-feedback-based formation control protocols were employed to achieve the maneuvering of the path-guided formation. Simulation results are shown in Figures 5–7. Figure 5a shows that the mobile robots were guided to follow the path with the commanded speed and reached the desired geometry shape under the proposed control protocol, where the asterisk indicates the initial positions of the mobile robots, and the triangle indicates the positions of the mobile robots at  $t = 5$  s and  $t = 15$  s, respectively. Figure 5b shows the evolution of the path parameter. It can be observed that the path-parameter-updating speed converged to a small neighborhood of the commanded speed. Figure 6 displays the curves of the mobile robots' states. It can be observed from Figure 6 that the formation position consensus errors of the four mobile robots, as well as the mobile robots' heading angle, linear velocity, and angular velocity, reached convergence in a finite time. Figure 7 shows the control inputs of the four mobile robots. It is observed that the proposed control protocol drove the multiple mobile robots to keep the desired formation and follow the desired path with the assigned speed. Thus, we can conclude that the proposed control protocol is effective and efficient.

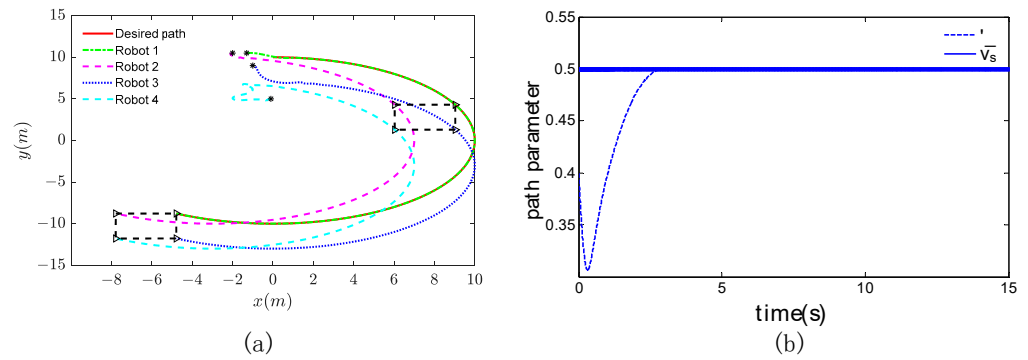


Figure 5. The trajectories of the NMRs (a) and evolution of the path parameter (b).

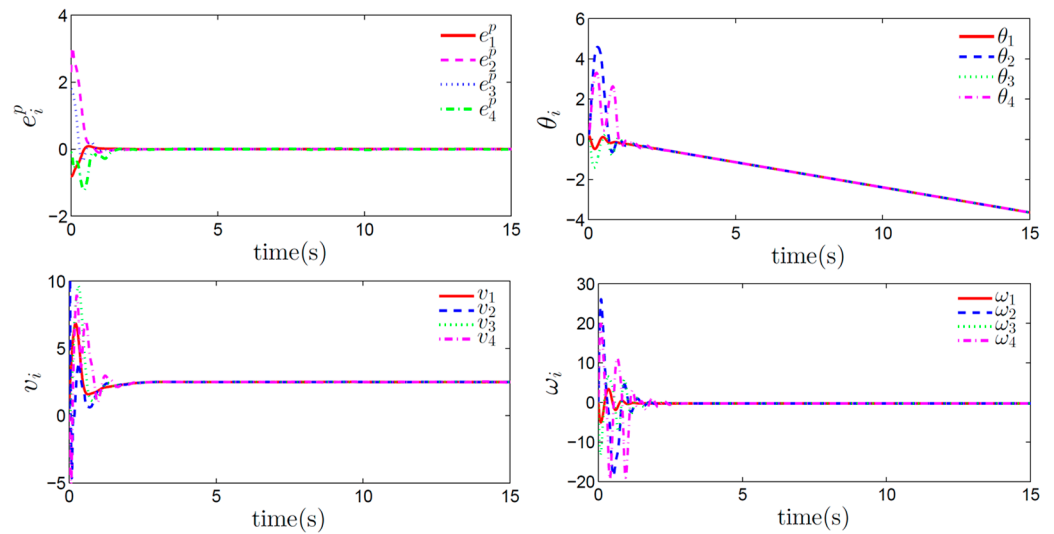


Figure 6. Evolutions of formation consensus errors, heading angles, linear velocities, and angular velocities of NMRs.

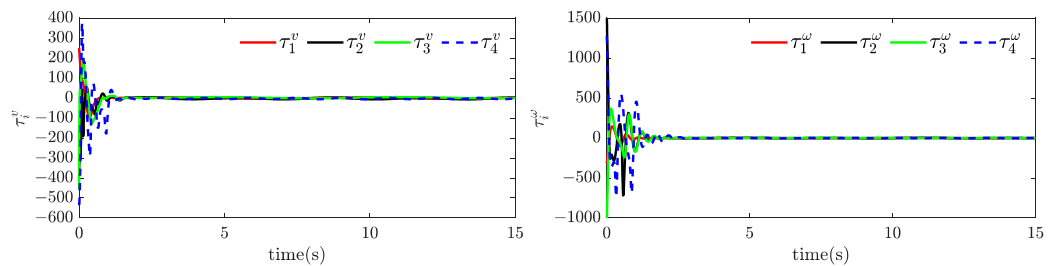


Figure 7. Control inputs of the NMRs.

### 5. Conclusions

In this paper, we investigated the output-feedback-based finite-time path-guided formation control of nonholonomic mobile robots. A finite-time extended state observer was designed to estimate the velocities and disturbances. Then, the formation control scheme consisting of kinematic control and dynamic control was proposed. For the kinematic control, a path-parameter-updating law was developed for a virtual leader, and the desired linear velocity and heading angle were developed for the mobile robots. For the dynamic control algorithm, an anti-disturbance control protocol was developed based on the estimated velocities and disturbances. The stability analysis of the closed-loop system was given, and simulation studies were conducted to demonstrate the effectiveness of the proposed control protocols.

**Author Contributions:** Conceptualization, Y.F., X.L. and S.L.; methodology, Y.F., X.L. and S.L.; software, Y.F.; validation, Y.F. and S.L.; formal analysis, Y.F., X.L. and S.L.; investigation, Y.F.; resources, Y.F.; data curation, Y.F. and S.L.; writing—original draft preparation, Y.F.; writing—review and editing, X.L. and S.L.; visualization, X.L., Z.J. and S.L.; supervision, X.L., Z.J., S.L. and B.G.; project administration, X.L. and B.G.; funding acquisition, X.L. and B.G. All authors have read and agreed to the published version of the manuscript.

**Funding:** This research was funded in part by the Natural Science Foundation of Hebei Province under Grant F2020202103, and the Scientific Research Program for Young Outstanding Talent of Higher Education of Hebei Province under Grant BJ2021045.

**Conflicts of Interest:** The authors declare no conflict of interest.

## References

1. Li, X.; Wen, C.; Chen, C. Adaptive Formation Control of Networked Robotic Systems with Bearing-Only Measurements. *IEEE Trans. Cybern.* **2020**, *51*, 199–209. [[CrossRef](#)] [[PubMed](#)]
2. Li, S.; Zhang, J.; Li, X.; Wang, F.; Luo, X.; Guan, X. Formation Control of Heterogeneous Discrete-Time Nonlinear Multi-Agent Systems with Uncertainties. *IEEE Trans. Ind. Electron.* **2017**, *64*, 4730–4740. [[CrossRef](#)]
3. Wang, J.; Luo, X.; Li, X.; Guan, X. Specified-time bearing-based formation control of multi-agent systems via a dynamic gain approach. *J. Frankl. Inst.* **2018**, *355*, 8619–8641. [[CrossRef](#)]
4. Ren, Y.; Sosnowski, S.; Hirche, S. Fully Distributed Cooperation for Networked Uncertain Mobile Manipulators. *IEEE Trans. Robot.* **2020**, *36*, 984–1003. [[CrossRef](#)]
5. Zhao, W.; Meng, Q.; Chung, P.W.H. A heuristic distributed task allocation method for multivehicle multitask problems and its application to search and rescue scenario. *IEEE Trans. Cybern.* **2016**, *46*, 902–915. [[CrossRef](#)]
6. Scherer, J.; Rinner, B. Multi-Robot Persistent Surveillance with Connectivity Constraints. *IEEE Access* **2020**, *8*, 15093–15109. [[CrossRef](#)]
7. Kanjanawanishkul, K. Coordinated Path Following for Mobile Robots Using a Virtual Structure Strategy with Model Predictive Control. *Automatika* **2014**, *55*, 287–298. [[CrossRef](#)]
8. Ghommam, J.; Mehrjerdi, H.; Saad, M.; Mnif, F. Formation path following control of unicycle-type mobile robots. *Robot. Auton. Syst.* **2010**, *58*, 727–736. [[CrossRef](#)]
9. Zhang, Q.; Lapiere, L.; Xiang, X. Distributed Control of Coordinated Path Tracking for Networked Nonholonomic Mobile Vehicles. *IEEE Trans. Ind. Inform.* **2012**, *9*, 472–484. [[CrossRef](#)]
10. Chen, X.; Huang, F.; Zhang, Y.; Chen, Z.; Liu, S.; Nie, Y.; Tang, J.; Zhu, S. A Novel Virtual-Structure Formation Control Design for Mobile Robots with Obstacle Avoidance. *Appl. Sci.* **2020**, *10*, 5807. [[CrossRef](#)]
11. Zhang, Y.; Wang, M. Coordinated path following control of multiple nonholonomic mobile robots with prescribed performance. In Proceedings of the 38th Chinese Control Conference, Guangzhou, China, 27–30 July 2019; pp. 5623–5628.
12. Cao, K.; Jiang, B.; Yue, D. Cooperative path following control of multiple nonholonomic mobile robots. *ISA Trans.* **2017**, *71*, 161–169. [[CrossRef](#)] [[PubMed](#)]
13. Wang, W.; Huang, J.; Wen, C. Prescribed performance bound-based adaptive path-following control of uncertain nonholonomic mobile robots. *Int. J. Adapt. Control Signal Process.* **2017**, *31*, 805–822. [[CrossRef](#)]
14. Zhao, Y.; Zhang, Y.; Lee, J. Lyapunov and Sliding Mode Based Leader-follower Formation Control for Multiple Mobile Robots with an Augmented Distance-angle Strategy. *Int. J. Control Autom. Syst.* **2019**, *17*, 1314–1321. [[CrossRef](#)]
15. Lin, S.; Jia, R.; Yue, M.; Xu, Y. On Composite Leader–follower Formation Control for Wheeled Mobile Robots with Adaptive Disturbance Rejection. *Appl. Artif. Intell.* **2019**, *33*, 1306–1326. [[CrossRef](#)]
16. Zhang, C.; Qin, W.; Fan, M.-C.; Wang, T.; Shen, M.-Q. A Q-Learning-Based Parameters Adaptive Algorithm for Formation Tracking Control of Multi-Mobile Robot Systems. *Complexity* **2022**, *2022*, 5093277. [[CrossRef](#)]
17. Xiao, W.; Zhou, Q.; Liu, Y.; Li, H.; Lu, R. Distributed Reinforcement Learning Containment Control for Multiple Nonholonomic Mobile Robots. *IEEE Trans. Circuits Syst. I Regul. Pap.* **2021**, *69*, 896–907. [[CrossRef](#)]
18. Yoo, S.J.; Park, B.S. Connectivity preservation and collision avoidance in networked nonholonomic multi-robot formation systems: Unified error transformation strategy. *Automatica* **2019**, *103*, 274–281. [[CrossRef](#)]
19. Xu, Y.; Wang, C.; Cai, X.; Li, Y.; Xu, L. Output-feedback formation tracking control of networked nonholonomic multi-robots with connectivity preservation and collision avoidance. *Neurocomputing* **2020**, *414*, 267–277. [[CrossRef](#)]
20. Li, Y.; Zhu, L.; Guo, Y. Observer-based multivariable fixed-time formation control of mobile robots. *J. Syst. Eng. Electron.* **2020**, *31*, 403–414. [[CrossRef](#)]
21. Hebertt, S.; Alberto, L.; Mario, R.; William, Z. *Active Disturbance Rejection Control of Dynamic Systems: A Flatness Based Approach*, 1st ed.; Butterworth-Heinemann: Oxford, UK, 2017.
22. Guo, B.; Zhao, Z. *Active Disturbance Rejection Control for Nonlinear Systems: An Introduction*, 1st ed.; John Wiley & Sons: Hoboken, NJ, USA, 2016; pp. 93–153.
23. Huang, Y.; Su, J. Visual Servoing of Nonholonomic Mobile Robots: A Review and a Novel Perspective. *IEEE Access* **2019**, *7*, 134968–134977. [[CrossRef](#)]

24. Liu, A.; Zhang, W.-A.; Yu, L.; Yan, H.; Zhang, R. Formation Control of Multiple Mobile Robots Incorporating an Extended State Observer and Distributed Model Predictive Approach. *IEEE Trans. Syst. Man, Cybern. Syst.* **2020**, *50*, 4587–4597. [[CrossRef](#)]
25. Chang, S.; Wang, Y.; Zuo, Z.; Yang, H. Fixed-Time Formation Control for Wheeled Mobile Robots with Prescribed Performance. *IEEE Trans. Control Syst. Technol.* **2021**, *30*, 844–851. [[CrossRef](#)]
26. Wang, N.; Zhu, Z.; Qin, H.; Deng, Z.; Sun, Y. Finite-time extended state observer-based exact tracking control of an unmanned surface vehicle. *Int. J. Robust Nonlinear Control* **2020**, *31*, 1704–1719. [[CrossRef](#)]
27. Ren, C.; Li, X.; Yang, X.; Ma, S. Extended State Observer-Based Sliding Mode Control of an Omnidirectional Mobile Robot with Friction Compensation. *IEEE Trans. Ind. Electron.* **2019**, *66*, 9480–9489. [[CrossRef](#)]
28. Li, P.; Yang, H.; Li, H.; Liang, S. Nonlinear ESO-based tracking control for warehouse mobile robots with detachable loads. *Robot. Auton. Syst.* **2021**, *149*, 103965. [[CrossRef](#)]
29. Ren, C.; Ding, Y.; Ma, S. A structure-improved extended state observer based control with application to an omnidirectional mobile robot. *ISA Trans.* **2020**, *101*, 335–345. [[CrossRef](#)] [[PubMed](#)]
30. Qin, B.; Yan, H.; Zhang, H.; Wang, Y.; Yang, S.X. Enhanced Reduced-Order Extended State Observer for Motion Control of Differential Driven Mobile Robot. *IEEE Trans. Cybern.* **2021**, 1–12. [[CrossRef](#)]
31. Zhu, Y.; Huang, Y.; Su, J.; Pu, C. Active disturbance rejection control for wheeled mobile robots with parametric uncertainties. In Proceedings of the 21st IFAC World Congress on Automatic Control—Meeting Societal Challenges, Berlin, Germany, 11–17 July 2020; pp. 1355–1360.
32. Lu, Q.; Chen, J.; Wang, Q.; Zhang, D.; Sun, M.; Su, C. Practical fixed-time trajectory tracking control of constrained wheeled mobile robots with kinematic disturbances. *ISA Trans.* **2022**. [[CrossRef](#)]
33. Hu, Q.; Jiang, B. Continuous Finite-Time Attitude Control for Rigid Spacecraft Based on Angular Velocity Observer. *IEEE Trans. Aerosp. Electron. Syst.* **2018**, *54*, 1082–1092. [[CrossRef](#)]
34. Aguiar, A.P.; Hespanha, J.P. Trajectory-Tracking and Path-Following of Underactuated Autonomous Vehicles with Parametric Modeling Uncertainty. *IEEE Trans. Autom. Control* **2017**, *52*, 1362–1379. [[CrossRef](#)]
35. Fukao, T.; Nakagawa, H.; Adachi, N. Adaptive tracking control of a nonholonomic mobile robot. *IEEE Trans. Robot. Autom.* **2000**, *16*, 609–615. [[CrossRef](#)]